Research Square

Preprints are preliminary reports that have not undergone peer review.
They should not be considered conclusive, used to inform clinical practice,
or referenced by the media as validated information.

Exceptional Bound States in the Continuum in a Passive Terahertz Metasurface

Chen Chen

22b911041@stu.hit.edu.cn

Harbin Institute of Technology https://orcid.org/0000-0002-6358-7289

Liu Ziyi

Harbin Institute of Technology

Jianfei Li

Harbin Institute of Technology

Zhou Junhan

Harbin Institute of Technology

Jiang Yuanhang

Harbin Institute of Technology

Ying Wang

Harbin Institute of Technology

Zhongxiang Zhou

Harbin Institute of Technology

Hongyu Liu

City University of Hong Kong https://orcid.org/0000-0002-2930-3510

Jingfeng Yao

Harbin Institute of Technology https://orcid.org/0000-0003-4094-9782

Gui-Geng Liu

Westlake University https://orcid.org/0000-0003-4328-9142

Chengxun Yuan

Harbin Institute of Technology https://orcid.org/0000-0002-2308-6703

Article

Keywords:

Posted Date: April 8th, 2026

DOI: https://doi.org/10.21203/rs.3.rs-9232537/v1

License: This work is licensed under a Creative Commons Attribution 4.0 International License.
Read Full License

Additional Declarations: There is **NO** Competing Interest.

Exceptional Bound States in the Continuum in a Passive Terahertz Metasurface

Chen Chen[1,#], Ziyi Liu[1,#], Jianfei Li[1,2,3,#,†], Junhan Zhou[1], Yuanhang Jiang[1], Ying Wang[1,2,3], Zhongxiang Zhou[1,2,3], Hongyu Liu [4], Jingfeng Yao[1,2,3,‡], Gui-Geng Liu[5,§], Chengxun Yuan[1,2,3,¶]

[1]School of Physics, Harbin Institute of Technology, Harbin 150000, China

[2]Heilongjiang Provincial Key Laboratory of Plasma Physics and Application Technology, Harbin 150000, China

[3]Heilongjiang Provincial Innovation Research Center for Plasma Physics and Application Technology, Harbin, 150001, China

[4]Department of Mathematics, City University of Hong Kong, Kowloon, Hong Kong SAR, China

[5]Department of Electronic and Information Engineering, School of Engineering, Westlake University, Hangzhou, 310030, China.

[#]These authors contributed equally to this work

[†‡§¶]corresponding author: jianfei_li@hit.edu.cn; yaojf@hit.edu.cn; liuguigeng@westlake.edu.cn; yuancx@hit.edu.cn

Exceptional bound states in the continuum (EP-BICs) are hybrid singularities in non-Hermitian systems that uniquely combine the non-radiating characteristic of bound states in the continuum (BICs) with the enhanced sensitivity of exceptional points (EPs). However, their experimental realization remains challenging because existing proposals typically require precise external excitation to control the loss and coupling strength. Here, we experimentally demonstrate an EP-BIC in a fully passive terahertz metasurface. Through simple geometric rotation, we modulate the internal coupling of two resonator modes to drive an isolated EP to coalesce with a line of BICs and finally form an EP-BIC, as clearly traced by transmission spectra measurements. Near-field terahertz scanning further observes the uniform phase distribution of EP-BIC, confirming its decoupling from incident light. Finally, the sensor performance of EP-BIC is demonstrated in water mist detection and exhibits a distinct dip response that enables unambiguous signal identification, in contrast to the weak and spectrally crowded peak of conventional EP. Our work establishes a practical and robust platform for EP-BICs, opening avenues for ultra-sensitive photonic sensing.

Introduction

Exceptional points (EPs) are spectral singularities in non-Hermitian systems where at least two eigenstates coalesce in both their eigenvalues and eigenvectors [1–4]. This coalescence results in the eigenvalue splitting that depends nonlinearly (e.g., square-root near a second order EP) on external perturbations strength that surpasses the linear sensitivity of conventional resonances [5, 6]. Thus, photonic systems operating near an EP exhibit strongly enhanced sensitivity, making them highly promising for next-generation optical sensing [7–9]. However, the performance of EP-based sensors, especially in nanophotonic or integrated resonator systems, is fundamentally constrained by radiative losses [10–12]. These losses contribute a dominant imaginary part to the complex eigenfrequencies, broadening the resonance linewidths and thereby obscuring the enhanced spectral splitting induced by small perturbations [13–15]. Consequently, the resulting signal might be difficult to be distinguished from noise due to its poor detectivity, making the full sensitivity potential of an EP unattainable in practical passive systems where radiation losses dominate the mode decay.

On the other hand, bound states in the continuum (BICs) represent another class of singularities in open systems [16]. They are non-radiative resonant states that arise from destructive far-field interference or symmetry protection, exhibiting theoretically infinite radiative quality (Q) factors and perfect energy confinement [17–21]. Crucially, recent theoretical proposals have explored the potential for several BICs to coalesce into an EP form of an exceptional bound state in the continuum (EP-BIC) [22–24]. Such a state would inherently combine the vanishing radiative losses of the BICs with the enhanced eigenvalue sensitivity of an EP, promising a breakthrough for ultra-sensitive photonic sensing [25–30]. Nevertheless,

51 despite several reports on the coexistence or mutual transition between EPs and BICs within
52 the same parameter space [31–34], a direct experimental realization of a genuine, coalescent EP-
53 BIC remains elusive. The main challenge is that the previous proposals [23, 31] rely on
54 simultaneous and independent tuning of the external excitation for loss fine-tuning and the
55 internal coupling between each resonant mode, which is extremely difficult to achieve reliably
56 in experiment due to the difficulty in accurately controlling material losses and fabrication
57 imperfections.

58 In this work, we report the first experimental realization of an EP-BIC singularity in a fully
59 passive terahertz metasurface, achieved without introducing external gain or loss. The unit of
60 the metasurface is composed of two metallic split-ring resonators (SRRs), each supporting a
61 distinct resonant mode. By rotating the inner ring, we geometrically tailor the internal coupling
62 between the two modes, which drives an isolated EP to coalesce with a line of BICs state,
63 thereby forming a unified EP-BIC. We trace this evolution through transmission spectra
64 measurements at various rotation angles, observing that the characteristic resonant peak at the
65 EP gradually vanishes as a dip when the system transitions into the nonradiative EP-BIC state.
66 Via near-field terahertz scanning technology, the energy of EP-BIC state is found to be localized
67 at the center of Brillouin zone, similar to conventional symmetry-protected BIC (S-BIC).
68 Furthermore, we observe from the phase-resolved measurements that the spatial phase
69 distribution of the EP-BIC is uniform, different from the conventional quasi-BIC (q-BIC),
70 providing direct evidence for its decoupling from incident wave. Finally, by introducing a
71 minute and reversible perturbation via water mist spraying on the metasurface, we demonstrate
72 that EP-BIC exhibits a distinct spectral dip than the complex peaks at EP, highlighting its

improved detectability in the spectral response. Our work establishes a fully passive platform for realizing EP-BICs and opens new avenues for ultrasensitive photonic sensors.

Results

Our designed metasurface is illustrated in Fig. 1(a), which consists of a two-dimensional array of metal SRRs embedded on a dielectric silicon nitride (Si_3N_4) substrate in Fig. 1(b). Each unit cell comprises two SRRs with radius r_o and r_i for the outer and inner ring, respectively. The outer ring has two splits that are symmetric with respect to the x-axis, whereas the inner ring has a single split oriented at an angle θ relative to the x-axis (Fig. 1(b)). The center of inner ring is offset from that of outer ring by a distance d along the positive x-direction. Here, only the terahertz wave polarized along the x-axis is considered. At a fixed rotation angle θ of the structure, Fig. 1(d) plots the numerically simulated real part of the eigenfrequencies by varying the offset distance d and the inner ring radius r_i. The black line depicts the eigenfrequencies at a fixed r_i where the "bulk Fermi arc" ($\omega_+ = \omega_-$) exists. The blue strip region indicates the states with ultra-low intrinsic loss, manifested as BICs state. At the rotation angle, a pair of EPs appears. It is found that the BICs state intersects with the "bulk Fermi arc", but does not intersect with the EPs. As we gradually rotate the inner SRRs to decrease the θ, one of the EPs moves towards the smaller d region (r_i remains unchanged at 68.87 μm) and finally merges with the BICs states, forming the pursued EP-BIC. To better understand the formation mechanism of our EP-BIC, we model our structure as an effective two-level Hamiltonian [35–37]:

$$H = \begin{pmatrix} \omega_1 - i\gamma_1 & \kappa' - i\gamma_0 \\ \kappa' - i\gamma_0 & \omega_2 - i\gamma_2' \end{pmatrix} \quad (1)$$

where the ω_1 and ω_2 respectively denote the resonance frequencies of the outer and inner SRR.

Here, γ_1, γ_2' ($\gamma_2' = \gamma_2 + \gamma_{\text{int}}$) represent the losses of the outer and inner SRR. The intrinsic loss γ_{int} of the inner SRR originates from the C_2 symmetry breaking [38–42]. The far-field and near-field coupling coefficients between two SRRs are given by $\gamma_0 = \sqrt{\gamma_1 \gamma_2'}$ and $\kappa' = \kappa + m\cos\theta$ respectively, where κ and m are assumed to be real. Here, κ' is related to the rotation angle θ, and κ is depended on the offset distance d between the two SRRs. The complex eigenvalues $\omega_\pm$ of this system can be derived as:

$$\omega_\pm = \bar{\omega} - i\bar{\gamma} \pm \Lambda \tag{2}$$

where $\Lambda = \sqrt{(\delta\omega - i\delta\gamma)^2 + (\kappa' - i\gamma_0)^2}$ with $\bar{\omega} = (\omega_1 + \omega_2)/2$,and $\bar{\gamma} = (\gamma_1 + \gamma_2 + \gamma_{\text{int}})/2$, $\delta\omega = (\omega_2 - \omega_1)/2$, $\delta\gamma = (\gamma_2 + \gamma_{\text{int}} - \gamma_1)/2$. The EP can be realized when $\Lambda = 0$ in Eq. (2), corresponding to the coalescence of two eigenvalues [37, 43]. For a single SRR with C_2 symmetry, it supports a S-BIC in which far-field radiation loss is fully suppressed, yielding $\gamma_{1,2} = 0$ [44, 45]. However, incorporating the unavoidable intrinsic loss $\gamma_{\text{int}} \neq 0$ even when the BICs conditions $\gamma_{1,2} = 0$ are satisfied, leading to a modified BICs condition given by $\kappa'^2 = (\omega_\pm - \omega_1)^2 \mp i(\omega_\pm - \omega_1)\gamma_{\text{int}}$ [46]. This system can simultaneously satisfy the EP conditions $2\kappa' = \pm\gamma_{\text{int}}$ with $\omega_1 = \omega_2$, here $\gamma_{\text{int}} = 0.06$, $\kappa = -0.03$ and $m = 0.06$ at $\theta = 0^\circ$. Notably, $\gamma_2 \neq 0$ when the rotation of the inner SRR breaks the mirror system symmetry [46]. Figure 1(e) plots the calculated eigenvalues of the Hamiltonian in the κ–$\delta\omega$ parameter space, which is equivalent to the $d - r_i$ parameter space in metasurface. Clearly, as we modulate the parameter θ, similar profile and properties exhibit in Fig. 1(d), leading to the formation of an EP-BIC at $\theta = 0^\circ$ [46].

Next, we fabricate a series of the terahertz metasurfaces performing different rotation angles and at the EP state [46], with their scanning electron microscopy (SEM) images shown in Fig. 2(a). Each sample contains an array of 20×20 SRRs integrated on a thin and low stress

Si_3N_4 layer, and is held by a silicon with drilled holes to enable the transmission of terahertz waves [46]. The transmission properties of the samples are carried out by a high-precision 3D terahertz scanning system operating in the frequency range of 0.26−0.4 THz, with the setup illustrated in Fig. 2(b). The sample is placed between two terahertz antennas connected to a terahertz vector network analyzer. Initially at $\theta = 90^{\circ}$, a transmission peak emerges at 0.373 THz between two resonance dips around 0.359 THz and 0.395 THz as shown in Fig. 2(c). The dips stem from the resonant responses of the inner and outer rings while the transparency window (corresponding to the peak) arises from the mutual interaction between SRRs, which is a typical feature of EPs [47]. As θ decreases, the peak reduces and finally vanishes at $\theta = 0^{\circ}$ due to the gradual closing of the radiative channel when the EP merges with BICs. This manifests the formation of the non-radiative EP-BIC since it cannot couple to incident light [23]. Figure 2(c) also shows the simulated transmission spectra, which are in good agreement with the measurements.

To further characterize the spatial properties of the EP-BIC, we map near-field electric field distributions by raster-scanning a terahertz receiver 1 mm above the sample with a spatial resolution of 100 μm (Fig. 3(a)). For comparison, we also fabricate and scan a metasurface hosting q-BIC state with geometrical parameters ($d = -12.5\mu$m, $r_i = 67.12\mu$m, $\theta = 90^{\circ}$) [46]. The Fourier transformed energy distributions in the momentum space of the two samples are presented in Fig. 3(b) and (c), respectively, demonstrating strong energy confinement near the center of the Brillouin zone for both EP-BIC and q-BIC states [46], which are similar to conventional symmetry-protected BIC. Figure 3(d)-(f) displays the corresponding phase profiles measured at 0.385 THz for the EP-BIC sample, the q-BIC sample, and a bare Si_3N_4

139 film, respectively. The EP-BIC exhibits an essentially uniform phase distribution, consistent
140 with its radiation-free property resulting from destructive interference that decouples it from
141 the incident wave. In contrast, both the q-BIC sample and the bare film show a distinct annular
142 phase pattern. This pattern originates from the non-ideal plane-wave emission of the terahertz
143 emitter, which introduces a position-dependent optical path difference ΔL (Fig. 3(a)). Because
144 the q-BIC and bare film remain coupled to the incident radiation, the transmitted wave carries
145 this spatially varying phase profile, which is directly captured by the terahertz receiver. These
146 results confirm the non-radiative property of the EP-BIC.

147 Finally, we validate the application potential of our EP-BIC metasurface in mist detection,
148 with the experimental setup illustrated in Fig. 4(a). We spray water mist directly onto the
149 samples and monitor their transmission spectra evolution. First, we spray water mist onto a bare
150 Si_3N_4 film without SRRs structures (Fig. 4(b)), showing that the water spray alone induces no
151 detectable spectral change. Upon spraying the metasurface samples, the resonant frequency of
152 the conventional EP (blue circles) shifts from 0.389 THz to 0.387 THz, and that of the EP-BIC
153 (orange circles) shifts from 0.383 THz to 0.355 THz (Fig. 4(b)), which are attributed to the local
154 refractive-index change caused by the water mist. However, as clearly shown in Fig. 4(b), the
155 resonant peak associated with the conventional EP is weak and often coexists with other
156 unavoidable spectral peaks, making it challenging to unambiguously identify the water mist
157 induced signal. In stark contrast, the EP-BIC metasurface produces a single and pronounced
158 transmission dip that remains well-isolated from neighboring spectral structures. This distinct
159 spectral signature enables direct and reliable recognition of water mist-induced frequency shifts,
160 even for minute amounts of water mist. Our results demonstrate that compared to the

conventional EP, the EP-BIC metasurface exhibits more pronounced, distinguishable, and reliable response characteristics in water mist detection, highlighting its significant potential as a high-performance sensor.

Conclusion

In conclusion, we experimentally demonstrate the existence of an EP-BIC singularity in a fully passive metasurface at terahertz region. Through simple geometric rotation, the internal coupling between the SRRs is modulated, enforcing the coalescence of the EP and BIC into an EP-BIC, which is clearly observed in the transmission spectra. Near-field terahertz scanning reveals the energy tightly confined at the center of momentum space and distinguishes non-radiative EP-BIC from conventional q-BICs by the uniform phase distribution, confirming its decoupling from the incident light. Importantly, a reversible method confirms the distinct dip response associated with the EP-BIC, which is significantly distinguished from the complex peaks of conventional EP to minor perturbations. This work provides a robust and simplified platform for realizing EP-BIC in practice, paving the way for its application in ultrasensitive nanochip sensors.

Material and methods

Fabrications

First, a 2-mm-thick pre-drilled and double-side polished crystalline silicon wafer is cleaned and coated with a low-stress Si_3N_4 film on both sides via low-pressure chemical vapor deposition. Next, a 30-nm-thick chromium layer is deposited to enhance interfacial adhesion, followed by the fabrication of a 200-nm-thick gold pattern using a lift-off process. Backside alignment lithography is then performed with a contact aligner, and reactive ion etching was used to etch

windows in the Si_3N_4 layer. Finally, the suspended Si_3N_4 membrane is released by wet etching of the Si substrate, resulting in a final metasurface with an area of approximately 1×1 cm^2, suspended over the holes in the Si substrate.

Measurements

The high-precision 3D terahertz scanning system consists of the following core components: a terahertz vector network analyzer (VNA) Ceyear 3674 series, a frequency extension module paired with the VNA that up-converts the instrument's microwave output to the terahertz frequency range via frequency mixing technology, a pair of high-gain and broadband terahertz horn antennas serving as the transmitter and receiver, and a high-precision 3D scanning platform comprising a high-precision electric displacement stage and a 3D scanning gantry connected to a computer for control. This platform enables precise movement of the sample along the *x,y,z* axes, with a maximum positioning accuracy of 100 μm.

Acknowledgments

This work is supported by the National Natural Science Foundation of China (NSFC, Contracts No. 12575213, 12505229 and U2541210), Heilongjiang Province Young Science and Technology Talent Support Program (No.2023QNTJ016), Natural Science Foundation of Heilongjiang Province of China （No.YQ2024A008), the China Radio Wave Propagation Research Institute Stable Support for Scientific Research Funding under Project (A251200020) and National Key R&D Program of China (No.2025YFF0512000).

Author contributions

C. C. and Z. L. performed the simulations and prepared the samples; C.C., Z. L., J. L., J. Y, and

J. Z. helped on experimental spectrum measurements; C.C., Z. L., J. L. and J. Y. helped on the measurement setup; C.C., Z. L., J. L., J. Y., G.G.L. and C. Y provided a constructive discussion on the idea and the manuscript. C.C., Z. L., J. L. and J. Y analyzed the data. C.C., Z. L., J. L., J. Y. and G.G.L wrote the manuscript; Y.W, H. L, Z. Z and C. Y supervised the project.

Data availability

The data that support the findings of this study are available from the corresponding authors upon reasonable request.

Conflict of interests

The authors declare no competing interests.

Reference

[1] Mohammad-Ali Miri and Andrea Alu`. Exceptional points in optics and photonics. *Science*, 363(6422):eaar7709, 2019.

[2] Bo Zhen, Chia Wei Hsu, Yuichi Igarashi, Ling Lu, Ido Kaminer, Adi Pick, Song-Liang Chua, John D Joannopoulos, and Marin Solja˘ci´c. Spawning rings of exceptional points out of dirac cones. *Nature*, 525(7569):354–358, 2015.

[3] Kohei Kawabata, Takumi Bessho, and Masatoshi Sato. Classification of exceptional points and non-hermitian topological semimetals. *Phys. Rev. Lett.*, 123(6):066405, 2019.

[4] Weibao He, Shun Wan, Yunlan Zuo, Siyang Hu, Ziheng Ren, Zhongyi Yu, Dongsheng Yang, Xiang'ai Cheng, Keyu Xia, Yuze Hu, Hui Jing, and Tian Jiang. Lossenabled chirality inversion in terahertz metasurfaces. *Phys. Rev. Lett.*, 134:106901, 2025.

[5] Jun-Hee Park, Abdoulaye Ndao, Wei Cai, Liyi Hsu, Ashok Kodigala, Thomas Lepetit, Yu-Hwa Lo, and Boubacar Kant´e. Symmetry-breaking-induced plasmonic exceptional points and nanoscale sensing. *Nat. Phys.*, 16(4):462–468, 2020.

[6] Weiyuan Tang, Kun Ding, and Guancong Ma. Realization and topological properties of third-order exceptional lines embedded in exceptional surfaces. *Nat. Commun.*, 14(1), 2023.

[7] Hossein Hodaei, Absar U Hassan, Steffen Wittek, Hipolito Garcia-Gracia, Ramy El-Ganainy, Demetrios N Christodoulides, and Mercedeh Khajavikhan. Enhanced sensitivity at higher-order exceptional points. *Nature*, 548(7666):187–191, 2017.

[8] Weijian Chen, S¸ahin Kaya Ozdemir, Guangming Zhao,¨ Jan Wiersig, and Lan Yang. Exceptional points enhance sensing in an optical microcavity. *Nature*, 548(7666):192– 196, 2017.

[9] Dongyang Yan, Alexander S Shalin, Yongxing Wang, Yun Lai, Yadong Xu, Zhi Hong Hang, Fang Cao, Lei Gao, and Jie Luo. Ultrasensitive higher-order exceptional points via non-hermitian zero-index materials. *Phys. Rev.Lett.*, 134(24):243802, 2025.

[10] Weibao He, Shun Wan, Yunlan Zuo, Siyang Hu, Ziheng Ren, Zhongyi Yu, Dongsheng Yang, Xiang'ai Cheng, Keyu Xia, Yuze Hu, Hui Jing, and Tian Jiang. Lossenabled chirality inversion in terahertz metasurfaces. *Phys. Rev. Lett.*, 134(10):106901, 2025.

[11] Soojeong Baek, Sang Hyun Park, Donghak Oh, Kanghee Lee, Sangha Lee, Hosub Lim, Taewoo Ha, Hyun Sung

Park, Shuang Zhang, Lan Yang, Bumki Min, and Teun Kim. Non-hermitian chiral degeneracy of gated graphene metasurfaces. *Light Sci. Appl.*, 12(1):87, 2023.

[12] Kai Bai, Tian-Rui Liu, Liang Fang, Jia-Zheng Li, Chen Lin, Duanduan Wan, and Meng Xiao. Observation of nonlinear exceptional points with a complete basis in dynamics. *Phys. Rev. Lett.*, 132(7):073802, 2024.

[13] Mark Lawrence, Ningning Xu, Xueqian Zhang, Longqing Cong, Jiaguang Han, Weili Zhang, and Shuang Zhang. Manifestation of pt symmetry breaking in polarization space with terahertz metasurfaces. *Phys. Rev. Lett.*, 113(9):093901, 2014.

[14] Chang Li, Ruisheng Yang, Xinchao Huang, Quanhong Fu, Yuancheng Fan, and Fuli Zhang. Experimental demonstration of controllable pt and anti-pt coupling in a non-hermitian metamaterial. *Phys. Rev. Lett.*, 132(15):156601, 2024.

[15] Xintong Shi, Hai Lin, Tingting Liu, Yun Shen, Rongxin Tang, Le Li, Junyi Zhang, Yanjie Wu, Shouxin Duan, and Chenhui Zhao. Polarization-controlled non-hermitian metasurfaces for ultra-sensitive terahertz sensing. *Laser Photonics Rev.*, 19(14), 2025.

[16] Chia Wei Hsu, Bo Zhen, A Douglas Stone, John D. Joannopoulos, and Marin Solja˘ci´c. Bound states in the continuum. *Nat. Rev. Mater.*, 1(9):1–13, 2016.

[17] Meng Kang, Shunping Zhang, Meng Xiao, and Hongxing Xu. Merging bound states in the continuum at off-high symmetry points. *Phys. Rev. Lett.*, 126(11):117402, 2021.

[18] Weimin Ye, Yang Gao, and Jianlong Liu. Singular points of polarizations in the momentum space of photonic crystal slabs. *Phys. Rev. Lett.*, 124(15):153904, 2020.

[19] Chia Wei Hsu, Bo Zhen, Jeongwon Lee, Song-Liang Chua, Steven G Johnson, John D Joannopoulos, and Marin Solja˘ci´c. Observation of trapped light within the radiation continuum. *Nature*, 499(7457):188–191, 2013.

[20] Kirill Koshelev, Sergey Lepeshov, Mingkai Liu, Andrey Bogdanov, and Yuri Kivshar. Asymmetric metasurfaces with high-q resonances governed by bound states in the continuum. *Phys. Rev. Lett.*, 121(19):193903, 2018.

[21] Zhaoxian Su, Yuxuan Yang, Bo Xiong, Ruize Zhao, Yongtian Wang, and Lingling Huang. Planar chiral metasurface based on coupling quasi-bound states in the continuum. *Adv. Opt. Mater.*, 12(16):2303195, 2024.

[22] Haoye Qin, Xiaodong Shi, and Haiyan Ou. Exceptional points at bound states in the continuum in photonic integrated circuits. *Nanophotonics*, 11(21):4909–4917, 2022.

[23] Adria` Cano´s Valero, Zoltan Sztranyovszky, Egor A Muljarov, Andrey Bogdanov, and Thomas Weiss. Exceptional bound states in the continuum. *Phys. Rev. Lett.*, 134(10):103802, 2025.

[24] Liyun Cao and Badreddine Assouar. Asymmetric elastic bound state in the continuum by an exceptional point. *Phys. Rev. Lett.*, 135:246301, 2025.

[25] Meng Kang, Tao Liu, CT Chan, and Meng Xiao. Applications of bound states in the continuum in photonics.
Nat. Rev. Phys., 5(11):659–678, 2023.

[26] Hatice Altug, Sang-Hyun Oh, Stefan A Maier, and Ji˘r´ı Homola. Advances and applications of nanophotonic biosensors. *Nat. Nanotechnol.*, 17(1):5–16, 2022.

[27] Ming Lun Tseng, Yasaman Jahani, Aleksandrs Leitis, and Hatice Altug. Dielectric metasurfaces enabling advanced optical biosensors. *ACS photonics*, 8(1):47–60, 2020.

[28] Quanlong Yang, Zhibo Yao, Lei Xu, Yapeng Dou, Lingli Ba, Fan Huang, Quan Xu, Longqing Cong, Jianqiang Gu, and Junliang Yang. Ultrasensitive terahertz fingerprint

289 retrieval with multiple-bic-enabled meta-sensors. *Laser Photonics Rev.*, 19(2):2400825,
290 2025.
291 [29] Chiara Schiattarella, Silvia Romano, Luigi Sirleto, Vito Mocella, Ivo Rendina, Vittorino
292 Lanzio, Fabrizio Riminucci, Adam Schwartzberg, Stefano Cabrini, and Jiaye Chen.
293 Directive giant upconversion by supercritical bound states in the continuum. *Nature*,
294 (626):765–771, 2024.
295 [30] Zi-Lan Deng, Feng-Jun Li, Huanan Li, Xiangping Li, and Andrea Alu`. Extreme
296 diffraction control in metagratings leveraging bound states in the continuum and
297 exceptional points. *Laser Photonics Rev.*, 16(6):2100617, 2022.
298 [31] Lei Wang, Hang Liu, Junwei Liu, Aoxuan Liu, Jialiang Huang, Qiannan Li, Hui Dai,
299 Caihong Zhang, Jingbo Wu, Kebin Fan, Huabing Wang, Biaobing Jin, Jian Chen, and
300 Peiheng Wu. Photoswitchable exceptional points derived from bound states in the
301 continuum. *Light Sci. Appl*, 14(1):377, 2025.
302 [32] Zhiling Zhou, Bin Jia, Nengyin Wang, Xu Wang, and Yong Li. Observation of perfectly-
303 chiral exceptional point via bound state in the continuum. *Phys. Rev. Lett.*, 130(11):116101,
304 2023.
305 [33] Wei Li, Cai Luo, Shibing Tian, RuiXuan Zheng, Guangzhou Geng, Haifang Yang, Baoli
306 Liu, Qinghua Song, Yang Guo, and Changzhi Gu. Topological band engineering in q-bics
307 and eps derived from visible range plasmons. *Nano Lett.*, 25(15):6117–6124, 2025.
308 [34] Shun Wan, Yuze Hu, Ran Huang, Shiru Song, Hui Yang, Weibao He, Siyang Hu, Ziheng
309 Ren, Zhongyi Yu, Yunlan Zuo, Yulong Zhang, Dongsheng Yang, Xiang’ai Cheng, Franco

Nori, Hui Jing, and Tian Jiang. Spin-selective topological effects without encircling exceptional points. *Phys. Rev. Lett.*, 136:053801, 2026.

[35] Wonjoo Suh, Zheng Wang, and Shanhui Fan. Temporal coupled-mode theory and the presence of non-orthogonal modes in lossless multimode cavities. *IEEE J. Quantum Electron.*, 40(10):1511–1518, 2004.

[36] A. Z. Devdariani, V. N. Ostrovskiˇi, and Yu. N. Sebyakin. Crossing of quasistationary levels. *J. Exp. Theor. Phys.*, 44:477, 1976.

[37] Adria` Can´os Valero, Zoltan Sztranyovszky, Egor A. Muljarov, Andrey Bogdanov, and Thomas Weiss. Exceptional bound states in the continuum. *Phys. Rev. Lett.*, 134:103802, 2025.

[38] Tianwen Qi, Feihu Song, Binggang Xiao, Yong Du, and Jianyuan Qin. Excitation and sensing application of dualbound states in the continuum in metallic terahertz metasurfaces. *Opt. Lasers Eng.*, 180:108287, 2024.

[39] H. Friedrich and D. Wintgen. Interfering resonances and bound states in the continuum. *Phys. Rev. A*, 32:3231– 3242, 1985.

[40] Chia Wei Hsu, Bo Zhen, A. Douglas Stone, John D. Joannopoulos, and Marin Soljacic. Bound states in the continuum. *Nat. Rev. Mater.*, 1(9), 2016.

[41] Jiaqi Niu, Liyun Zhen, Jingquan Liu, and Bin Yang. Metasurface demonstration of exceptional points partitioned by a line of bound states in the continuum. *Phys. Rev. B*, 109:L241302, 2024.

[42] Jiaqi Niu, Jingquan Liu, and Bin Yang. Chirality enhancement and topological dynamics of vectorial bound states in the continuum across structural parameter space. *Opt. Lett.*, 50(12):3962–3965, 2025.

[43] Jiaqi Niu, Liyun Zhen, Jingquan Liu, and Bin Yang. Metasurface demonstration of exceptional points partitioned by a line of bound states in the continuum. *Phys. Rev. B*, 109(24):L241302, 2024.

[44] Jiaju Wu, Xiaotian Xu, Xiaoqiang Su, Song Zhao, Chao Wu, Yong Sun, Yunhui Li, Feng Wu, Zhiwei Guo, Haitao Jiang, et al. Observation of giant extrinsic chirality empowered by quasi-bound states in the continuum. *Phys. Rev. Appl.*, 16(6):064018, 2021.

[45] Longqing Cong and Ranjan Singh. Symmetry-protected dual bound states in the continuum in metamaterials. *Adv. Opt. Mater.*, 7(13):1900383, 2019.

[46] See supplemental material,for details (i) conditions for general bics,(ii) theoretical realization of ep-bic, iii theoretical and simulated analyze of an ep-bic in a passive metasurface, (iv) fabrication and geometric parameters of the metasurface, (v) a near-field terahertz scanning method for energy measurement in the momentum space, (vi) evaluation of ep-bic sensing characteristics using a non-destructive water mist spray method.

[47] Changqing Wang, Xuefeng Jiang, Guangming Zhao, Mengzhen Zhang, and Lan Yang. Electromagnetically induced transparency at a chiral exceptional point. *Nat. Phys.*, 16(25):1–7, 2020.

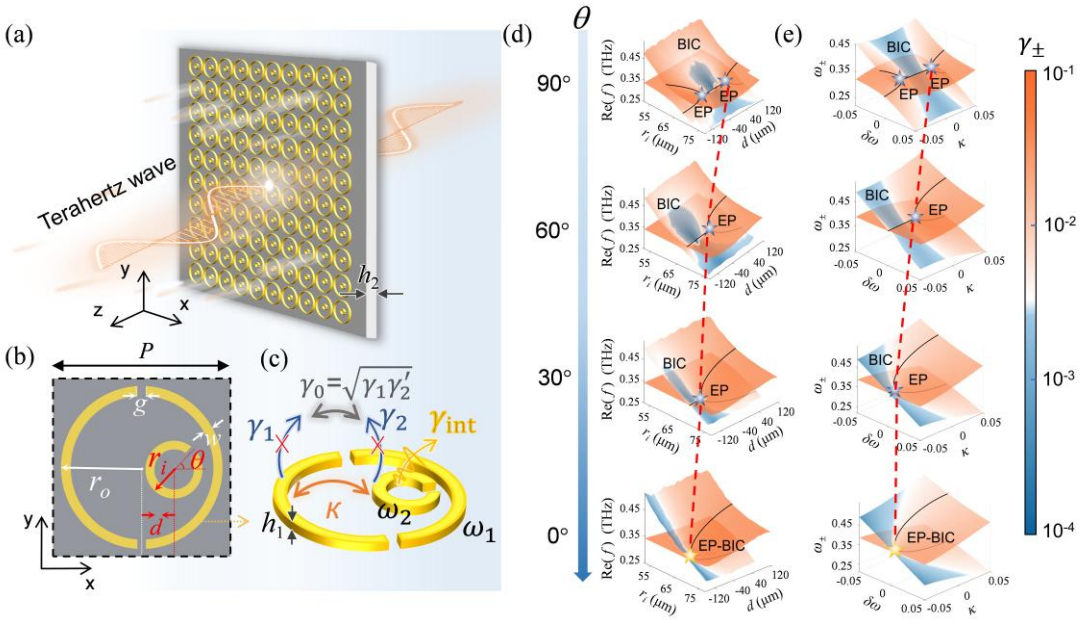
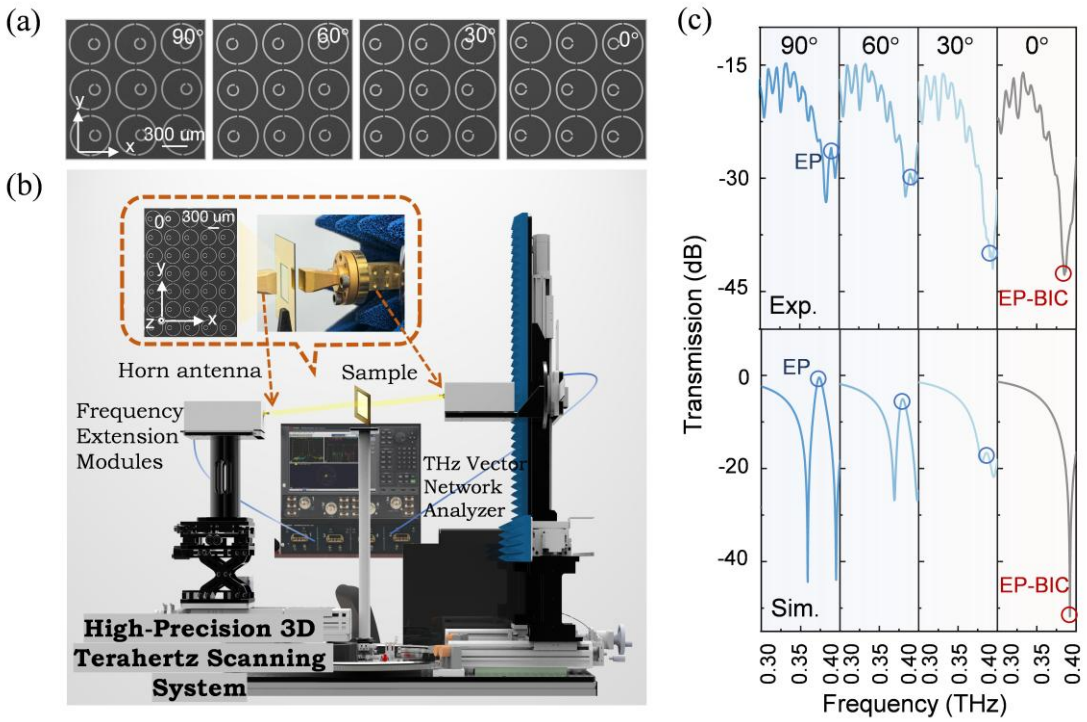


FIG. 1. **Design of metasurfaces performing an EP-BIC.** (a) Schematic illustration of the metasurface under x-polarized terahertz wave. (b)-(c) Illustration of the unit cell. P = 500μm, r_o = 225μm, w = 18.75μm, g = 18.75μm, r_i = 68.87μm, h_1 = 200nm, h_2 = 780nm. (d)-(e) Eigenfrequencies and eigenvalues of the SRRs metasurface in the d–r_i space and the effective Hamiltonian H in the $\kappa - \delta\omega$ space, respectively. The color manifests their imaginary part $\gamma_\pm$. The blue and yellow star indicates the EP and EP-BIC singularities, respectively. Red lines trace the evolution trajectories of an EP into an EP-BIC.



357

358 FIG. 2. **Experimental setup and measurement of transmission spectra.** (a) Scanning

359 electron microscopy (SEM) image of the fabricated metasurfaces with different geometric

360 parameters. (b) Schematic of high-precision 3D terahertz scanning system. The inset illustrates

361 experimental setup for transmission spectrum measurement. (c) Measured and simulated

362 transmission spectra, revealing the spectral evolution as the system transitions from the EP to

363 EP-BIC.

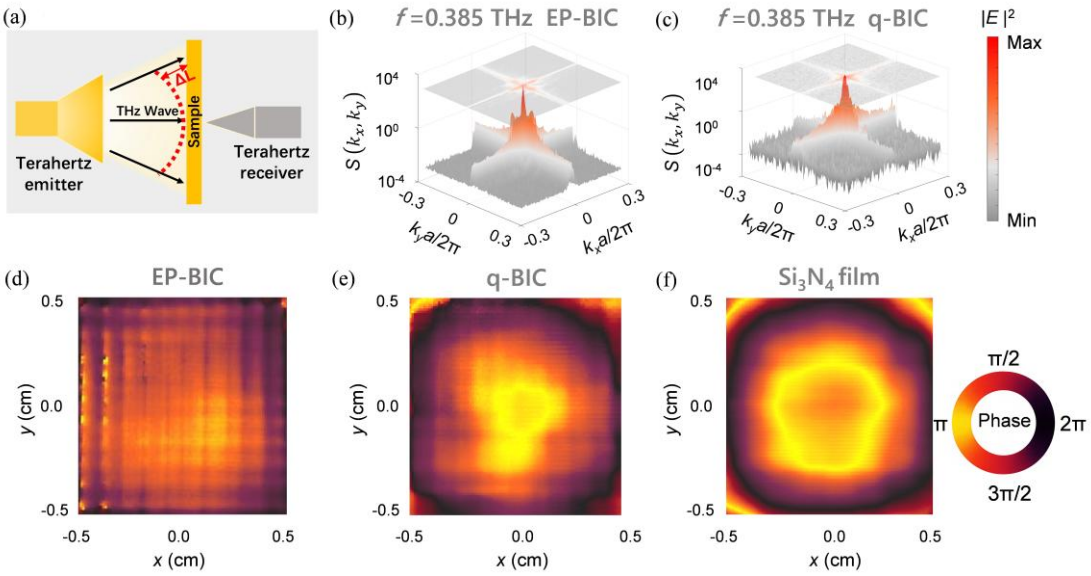
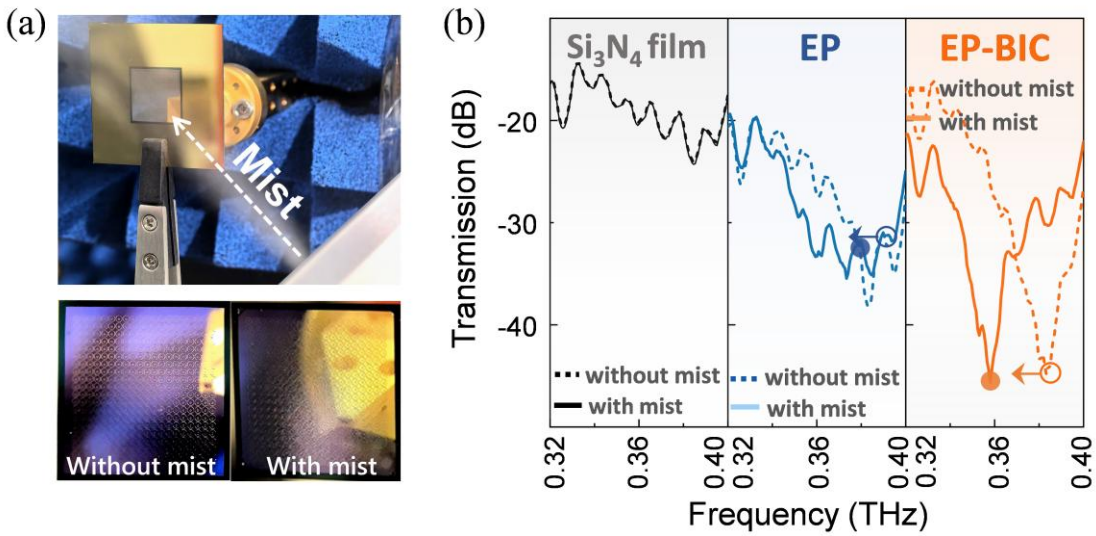


FIG. 3. **Characterization of the spatial properties of the EP-BIC.** (a) Schematic of the near-field scanning system. Energy distribution in the momentum space of (b) EP-BIC and (c) q-BIC, colored by the energy distribution. (d)-(f) Measured phase profile of the EP-BIC sample, the q-BIC sample, and the Si_3N_4 film at 0.385 THz, respectively.



369

370 FIG. 4. **Characterization of sensing performance of EP-BIC singularity.** (a) Experimental

371 setup and sample. Below are the photos of samples before and after the water mist spraying. (b)

372 Measured spectral transmission of the Si_3N_4 film, the EP sample, and the EP-BIC sample.

Supplementary Files

This is a list of supplementary files associated with this preprint. Click to download.

- veido.mp4
- SupplementalMaterialofExceptionalBoundStatesinthecontinuuminapassiveterahertzmetasurface.pdf